


SCIENTIFIC REPORTS



OPEN

Oxygen/phosphorus co-doped porous carbon from cicada slough as high-performance electrode material for supercapacitors

Bingwei Chen^{1,2}, Wenzhuo Wu³, Chunyang Li¹, Yanfang Wang^{1,2}, Yi Zhang¹, Lijun Fu¹, Yusong Zhu¹, Lixin Zhang² & Yuping Wu^{1,2} 

Synthesizing high-performance electrode materials plays a vital role in fabricating advanced supercapacitors. Heteroatom doping has been proved to be effective in enhancing the electrochemical properties of carbon-based electrodes. Herein, we report an O, P co-doped porous carbon (PC) originated from waste biomaterials, cicada sloughs. The PC possesses meso-/microporous structure with a large specific surface area ($1945 \text{ m}^2 \cdot \text{g}^{-1}$) and a high O, P co-doping ratio of 18 wt.%. These superior factors together enable it to deliver high specific capacitance ($295 \text{ F} \cdot \text{g}^{-1}$ in 6 M KOH and $291 \text{ F} \cdot \text{g}^{-1}$ in 1 M H_2SO_4), good cycling stability (100% capacitance retention after 10000 cycles in 1 M H_2SO_4) and rate performance. Therefore, from the respects of environment friendliness and cost effectivity, obtaining heteroatom doped carbons from the nature might be better compared to pyrolyzing heteroatom-containing chemicals.

Recently, due to the climate change and depletion of fossil fuels, developing high-performance, low cost and environmentally-friendly energy storage and conversion systems is of great significance^{1,2}. Because supercapacitors could deliver high power densities and long cycle lives ($>10^5$), they are regarded as promising devices bridging the power/energy gap between dielectric capacitors and traditional batteries³⁻⁵. Depending on the charge storage mechanism, supercapacitors can be classified into pseudo-capacitors and electrical double layer capacitors (EDLCs)³. Pseudo-capacitors store charges by fast and reversible redox reactions between the electrolyte and electrode materials, which allow them to deliver high energy densities comparable to those of batteries⁶. However, hindered by drawbacks such as poor cycling stability and low conductivity, they are not ideal for practical applications yet. As for EDLCs, they store energy through pure electrostatic charge accumulation occurring at the electrode/electrolyte interfaces, which means that they could store and release charges fast⁷. Because the capacitances and rate properties are dependent on specific surface area (SSA), pore size, electrical conductivity and wettability, porous carbons (PC) including activated carbons (AC), ordered mesoporous carbons (OMC), carbon nanotubes (CNT) and graphene are used exclusively in EDLCs⁸⁻¹⁰.

Among them, ACs have drawn wide attention owing to their controllable pore size, high SSA ($>1000 \text{ m}^2 \cdot \text{g}^{-1}$), large pore volume ($>0.5 \text{ cm}^3 \cdot \text{g}^{-1}$), excellent thermal stability and low cost¹¹. Traditional ACs, with SSA of more than $3000 \text{ m}^2 \cdot \text{g}^{-1}$, always show undesirable capacitances for EDLCs because of the sluggish ion diffusion in narrow micropores. Also, their poor electronic conductivity and long ion pathway induce high internal resistance and inferior rate performance.

In the past years, fabricating hierarchical and surface functionalized structures has been proved to be effective in improving their properties. For example, unlike traditional activation using KOH, ZnCl_2 or H_3PO_4 as the chemical activating agents. Xu *et al.* reported a meso-/microporous carbon with high percentage of mesopores of 52% through a dual-activation strategy¹². In addition to creating mesopores directly, introducing mesoporous

¹State Key Laboratory of Materials-oriented Chemical Engineering & School of Energy Science and Engineering, Nanjing Tech University, Nanjing, 211816, China. ²New Energy and Materials Laboratory (NEML), Department of Chemistry and Shanghai Key Laboratory of Molecular Catalysis and Innovative Materials, Fudan University, Shanghai, 200433, China. ³Guanghua Cambridge International School, Shanghai, 201315, China. Correspondence and requests for materials should be addressed to L.F. (email: l.fu@njtech.edu.cn) or Y.Z. (email: zhuys@njtech.edu.cn) or Y.W. (email: wuyup@njtech.edu.cn)

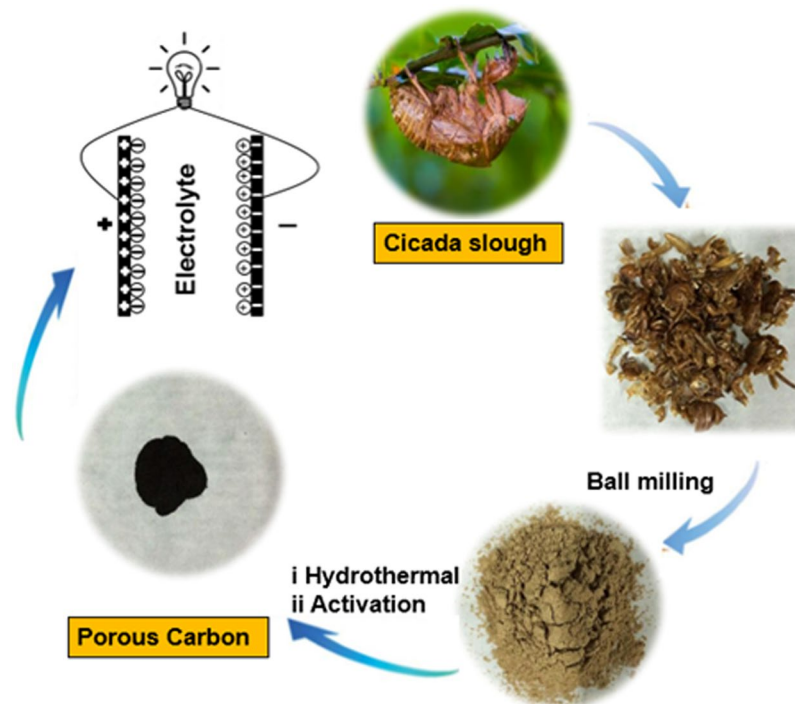


Figure 1. Illustration of the preparation process of the PC.

materials such as graphene and carbon nanotube as substrates for PCs could also construct rational structures¹³. Those materials showed enhanced electrochemical properties thanks to their hierarchical structures. Besides, tuning physiochemical and electronic properties of PCs by heteroatomic doping is a promising approach to fulfilling the requirements for high-performance supercapacitors^{14,15}. Through introducing defects into the lattice and altering the electron distribution, heteroatoms such as oxygen (O), fluorine (F), nitrogen (N), sulfur (S), phosphorus (P) and boron (B) could provide sites for specific adsorption and improve wetting property, which will further induce extra pseudo-capacitance and promote charge mobility in the doped PCs. In most cases, heteroatoms were introduced artificially by adding organic agents into carbon sources. For example, melamine and triphenylphosphine (TPP) are typical agents used for N and P doping, respectively. Although fabricating hierarchical structures and doping from chemical agents could provide materials with enhancing properties, achieving those goals in more cost-effective ways is of great importance as far as practical application is concerned.

So far, a variety of precursors such as fossil materials, polymers and waste biomaterials have been applied to produce ACs^{16–20}. Among them, waste biomaterials have attracted strong interests thanks to their renewability, readily availability, economic and environmental friendliness^{21,22}. For instance, the PC prepared via activation of shiitake mushroom shows high specific capacitances in a three-electrode system²³. The PC microflakes originating from willow catkins deliver specific capacitance of 233.1 F·g⁻¹ at 1 A·g⁻¹ and exhibit 82.9% capacitance retention at 20 A·g⁻¹ in 2 M KOH²⁴. Therefore, exploring high-performance PCs from the nature is of great promise.

Herein, we report a P, O co-doped carbon with meso-/microporous structures derived from cicada slough, a widely distributed biomass-waste in summer. After activation, cicada sloughs, rich in amino acid, protein, chitin, P and some microelements, converted into a surface functionalized meso-/microporous carbon. It shows a high SSA of 1945 m²·g⁻¹ and a O, P co-doping amount of more than 18 wt.%. Thanks to its rational porous structure and heteroatoms doping, when tested as electrode material for supercapacitors, the as-prepared PC presents higher specific capacitance, excellent rate and cycling performance in both acid and alkaline solutions.

Results

The preparation of the cicada sloughs-based PC is illustrated in Fig. 1. The approaches to converting ball-milled cicada sloughs into PC include hydrothermal treatment and the followed pyrolysis taking H₃PO₄ as the activation agent. For comparison, the hydrothermal product was pyrolyzed directly without H₃PO₄ and named PC_{untreated}. The details are shown in the Methods section.

As shown in Fig. 2a, direct pyrolysis produced irregular carbon particles attached with lots of scattered small particles. However, those small particles were removed in the existence of H₃PO₄, exposing rough surfaces caused by the formation of large amounts of pores (Fig. 2b). Besides, according to the EDX results, some elements including Al, Mg, Ca and Si existed in PC_{untreated} and disappeared in PC, revealing that H₃PO₄ not only acted as pore creator but also scavenger for impure components.

The TEM image (Fig. 2c) reveals that meso/microporous channels have been created successfully through activation. The uniform distributed meso/microporous structure of PC is beneficial to enhancing its electrochemical performances. Since the micropores can provide abundant sites to store charges and the inter-knit mesopores

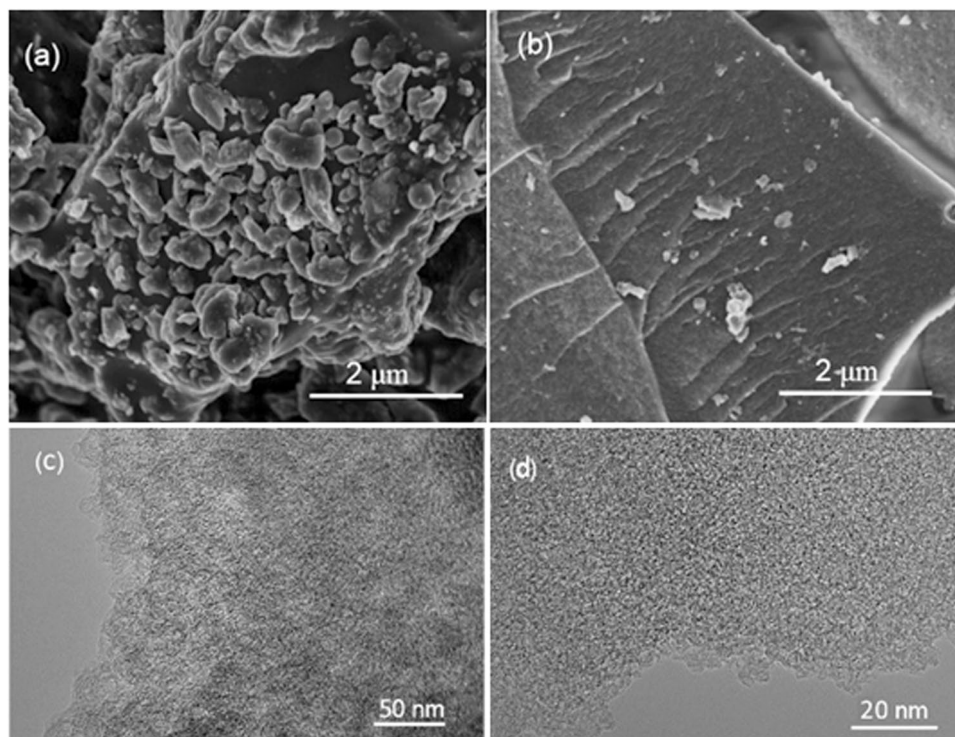


Figure 2. SEM images of (a) $PC_{\text{untreated}}$ and (b) PC, and (c,d) TEM images of PC.

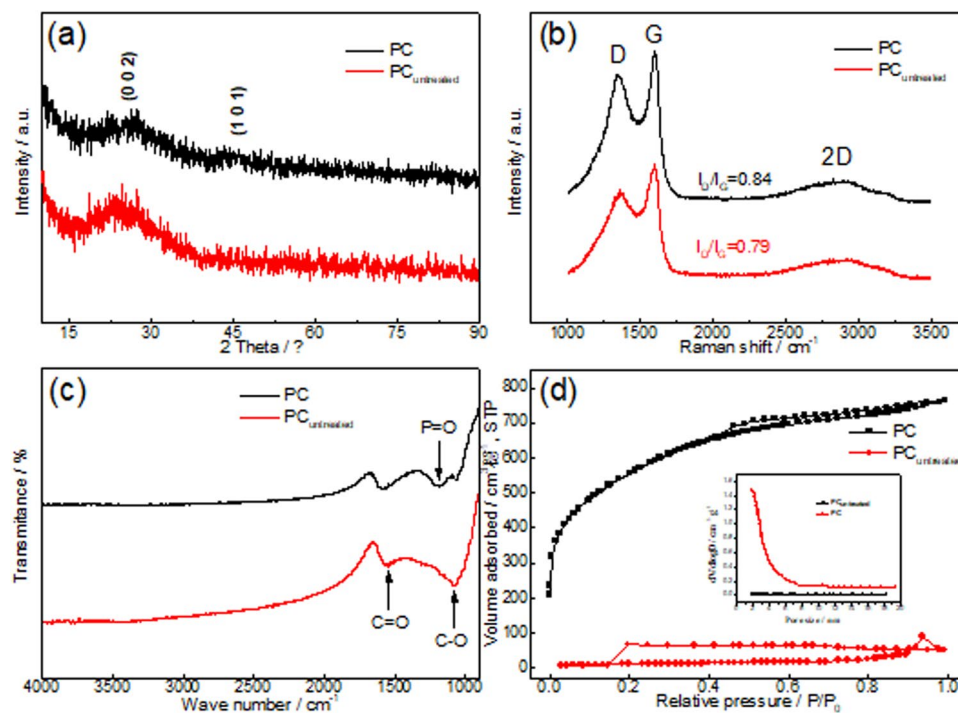


Figure 3. (a) XRD patterns, (b) Raman spectra, (c) FTIR spectra and (d) N_2 adsorption-desorption results of PC and $PC_{\text{untreated}}$.

can facilitate ion transportation, the diffusion distance from mesopores to micropores could be shortened, enabling improved capacitance and fast response²⁵. The disordered graphene-type structures observed at the edge of the PC (Fig. 2d) could promote electron transfer and lower intrinsic resistance¹⁶.

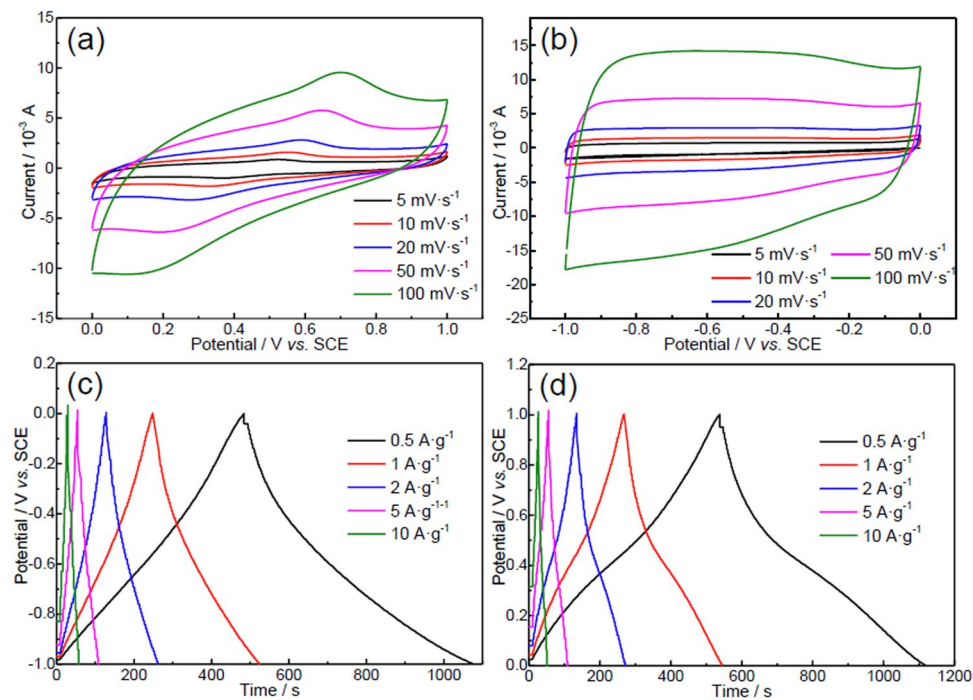


Figure 4. CV curves of the PC in (a) 1 M H₂SO₄ and (b) 6 M KOH, and its charge-discharge curves in (c) 1 M H₂SO₄ and (d) 6 M KOH.

Two broad peaks centered at $2\theta = 25$ and 46° in both XRD patterns of the PC and PC_{untreated} (Fig. 3a), corresponding to the (002) and (101) planes of graphite, respectively, indicate their low crystallinities²⁶. As shown in Fig. 3b, both of their Raman spectra exhibit two specific peaks at 1365 (D band) and 1600 cm⁻¹ (G band), relating to disordered carbon and sp²-bonded carbons, respectively²⁷. The increased relative intensity of D and G bands (I_D/I_G) in the PC (0.84) implies that the H₃PO₄ activation could not only open closed pores but also etch graphitized carbon to create more disordered structures²⁸.

Besides, with the help of H₃PO₄, more oxygen-containing functional groups were formed in the PC sample (Fig. 3c). For the PC_{untreated} sample, as shown in its FTIR spectra, two peaks at 1100 and 1630 cm⁻¹ could be attributed to C-O and C=O stretches. Although it contains similar amount of phosphorus (4.87 wt.%) to that in the PC sample (4.58 wt.%), no peak belonging to C-P-O linkage is observed. However, for the PC sample, its FTIR spectra show a new peak at 1180 cm⁻¹, which could be assigned to the stretching vibration of P=O groups²⁹. In some formerly reported papers, H₃PO₄ activation could introduce P to ACs, but usually on a smaller level¹¹. Therefore, in this case, the P-heteroatoms in P=O groups might come from both the H₃PO₄ and the existed P in carbon matrix, C-P=O³⁰. Since the electronegativity of P (2.19) is lower than that of C (2.55), the existed P-heteroatoms are inclined to be functionalized by acid-oxidizing, a common way of getting surface functionalized carbons. Because of the inherently hydrophobic nature of carbon matrix, ion transportation inside the microporous structures is always unsatisfying. Those oxygen-containing functional groups on the material surfaces could improve their wettability, promote ion transfer and provide extra pseudo-capacitance²⁷.

According to the N₂ adsorption-desorption isotherms (Fig. 3d), the PC exhibits combined I/IV types adsorption-desorption isotherms (according to the IUPAC classification) with an apparent hysteresis loop at a wide relative pressure between 0.4 and 1.0, indicating the coexistence of micropores and mesopores. Also, thanks to H₃PO₄ activation creating large amounts of new pores, the PC presents higher Brunauer-Emmett-Teller (BET) surface (S_{BET}) (1945 m²·g⁻¹) and larger total pore volume (V_{tot}) (1.184 cm³·g⁻¹) than those of the PC_{untreated} (35.5 m²·g⁻¹ and 0.07 cm³·g⁻¹, respectively). The high S_{BET} and V_{tot} are beneficial to the electrochemical performance since they can ensure more ions adsorption sites and more interconnected ion diffusion pathways that favor ion transport into/from the PC electrode material³¹. According to their Barrett-Joyner-Halenda (BJH) pore size distribution plots (the inset of Fig. 3d), after the activation, the average pore diameter (D_{av}) decreases from 43.9 nm (PC_{untreated}) to 2.81 nm, suggesting that the activating agent creates a great deal of micropores and mesopores.

As shown in Fig. 4a, the CV curves of the PC electrode in 1 M H₂SO₄ show a pair of peaks corresponding to the emergence of pseudo-capacitance (Fig. 4a), indicating that those surface functionalized groups, acting as favorable binding sites, significantly enhance its binding affinity toward H⁺. Also, a pair of broad peaks are observed in its CV curves when tested in alkaline solution (6 M KOH), which might be attributed to the specific adsorption of OH⁻ on C-P=O sites (Fig. 4b). Thanks to the functionalized groups and meso-/microporous structure of the PC, its CV curves still retain regular shapes at high potential scan rates, revealing its good rate performances in both acid and alkaline solutions. The symmetric charge-discharge curves at various current densities also indicate its good rate performance and electrochemical reversibility in those solutions (Fig. 4c,d).

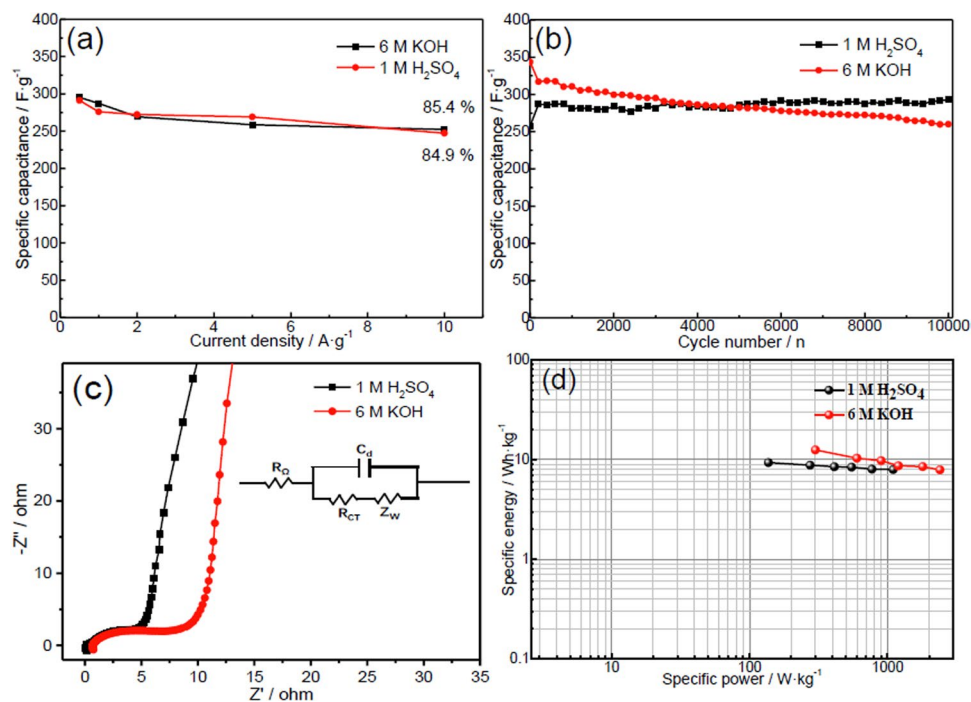


Figure 5. (a) Rate performance, (b) cycling stability and (c) Nyquist plots of the PC in acid and alkaline solutions; (d) Ragone plots of symmetric supercapacitors in 1 M H₂SO₄ and 6 M KOH (inset is equivalent electric circuit).

The specific capacitance was calculated from the discharge curves according to the following equation:

$$C_s = \int \frac{Idt}{m dV} \quad (1)$$

where C_s is the specific capacitance (F·g⁻¹), I is the discharge current (A), dt is the differential of discharge time, m is the mass of the active materials (g) and dV (V) is the differential of potential. As shown in Fig. 5a, the PC could deliver specific capacitances of 295.3 and 291.2 F·g⁻¹ at 0.5 A·g⁻¹ in 6 M KOH and 1 M H₂SO₄ electrolytes, respectively, which are superior to those of many biomaterial-derived carbons (Table S1)^{29,32–40}. Although ion diffusing into the inner micropores is limited by the short time at high current density, its specific capacitances still maintain at 252 (6 M KOH) and 247 F·g⁻¹ (1 M H₂SO₄) at 10 A·g⁻¹, with capacitance retention of 85.4% and 84.9%, respectively. Its high capacitance and good rate stability can be attributed to the following factors: (1) the ultrahigh SSA and pore volume accommodating ions; (2) the well-connected meso-/microporous network enabling the thorough utilization of surface and fast ion transportation; and (3) the surface functionalized groups especially the doping of O and P inducing pseudo-capacitance and enhanced wettability^{30,41}.

The cycling performance of the PC was conducted at the current density of 1 A·g⁻¹ (Fig. 5b). In H₂SO₄ solution, the capacitance of PC increases during the initial 200 cycles because the H⁺ penetrating from the surface to the near-surface bodies could contribute to extra pseudo-capacitance⁴¹. However, in KOH solution, since OH⁻ could not infiltrate into the bodies easily because of its large size and its same electrical property with that of oxygen-containing groups repulsing each other, no activation process is observed. After 10000 cycles in H₂SO₄ solution, its capacitance remains at about 287 F·g⁻¹ with no capacitance decay. In contrast, it falls 24% over 10000 cycles in KOH solution. This phenomenon is resulted from the pseudo-capacitance contribution of oxygen-containing functional groups, which is smaller in alkaline solution than that in acid solution, and those functional groups are not very stable in alkaline solutions⁴². If there is no functional groups, the AC will present stable cycling.

The differences of its electrochemical performances in acid and alkaline solutions could also be drawn from its EIS results in those solutions (Fig. 5c). The overall resistance of an electrode (resistance at the “knee” point, R_{knee}) can be determined by the extrapolation of the capacitive line to the 45° line. The relationship between various resistances follows the equations below.

$$R_{knee} = R_\Omega + R_p + R_D \quad (2)$$

$$R_{ct} = R_p + R_D \quad (3)$$

The internal resistance of an electrode (notated as R_Ω) could be obtained from the point intersecting with real axis at high frequency. The polarization resistance (R_p), i.e. the diameter of semicircle, reveals penetrating ability of electrolyte into porous electrode. The diffusional resistance (R_D), i.e. the length of 45° line in middle frequency

region, indicates migration rate of ions from electrolyte inside pores to the surface of electrode. The lower charge transfer resistance ($R_{ct} \approx 4.1 \Omega$) in H_2SO_4 solution reveals that H^+ could transfer easily in O, P-codoped porous carbons thanks to its smaller size and its different electrical property with that of oxygen-containing groups inducing smooth ion transfer. Besides resistances, the straight line in low frequency region is an important measurement of capacitive behavior and a vertical line suggests ideal capacitive performance. From this perspective, the PC electrode demonstrates better capacitive behavior in KOH solution because the capacitance mostly draws from electrochemical double-layers.

To further investigate the practical applicability of the PC, symmetric supercapacitors based on the PC in 6 M KOH and 1 M H_2SO_4 were assembled. The energy and power densities of the symmetrical supercapacitor systems were calculated according to the following equations:

$$E = \frac{C \int V^2 dV}{2} \quad (4)$$

$$P = E/t \quad (5)$$

where E ($Wh \cdot kg^{-1}$) is the specific energy density, P ($W \cdot kg^{-1}$) is the specific power density, C ($F \cdot g^{-1}$) is the specific capacitance of the total symmetrical system, V is the potential (V), and t is the discharge time (s). On the basis of the weights of the two electrodes, the specific energy densities are $12.5 Wh \cdot kg^{-1}$ at the power density of $300 W \cdot kg^{-1}$ in 6 M KOH and $9.32 Wh \cdot kg^{-1}$ at $137 W \cdot kg^{-1}$ in 1 M H_2SO_4 (Fig. 5d), which are superior to those of previously reported biomass-derived carbon materials, such as rice husk-derived PC ($8.36 Wh \cdot kg^{-1}$)⁴³, a PC prepared by chicken feather ($4.77 Wh \cdot kg^{-1}$)⁴⁴, and highly porous activated carbon electrodes from fibers of oil palm empty fruit bunches ($4.297 Wh \cdot kg^{-1}$)⁴⁵. Those results demonstrate that this PC-based supercapacitor is of great promise for practical applications.

Discussion

Just like harvesting energy from the sun, obtaining materials from the nature for practical applications is the thing that human beings have kept doing for thousands of years. Only when human learn and get inspired from the nature thoroughly could we innovate more incredible things. In the past years, fabricating hierarchical structure and heteroatom doping have been regarded as typical methods to improve the electrochemical properties of carbon-based materials. In this paper, we demonstrate that doping from the nature is an effective way of getting high-performance porous carbons⁴¹.

In summary, a porous carbon (PC) with high specific surface area, oxygen-containing groups and doped heteroatoms was prepared from cicada sloughs through pyrolysis and H_3PO_4 activation. The PC shows meso-/microporous structures with a high specific surface area ($1945 m^2 \cdot g^{-1}$) and a O, P co-doping ratio up to 18 wt.%. The doping effects of O and P on the capacitance is similar to those in carbon for lithium ion batteries, which lead to an increase of capacitance⁴¹. Of course, further detailed investigation should be investigated since different situation perhaps would result in different effects. Here, it exhibits excellent electrochemical performances, namely, high specific capacitances of 295 (6 M KOH) and 291 $F \cdot g^{-1}$ (1 M H_2SO_4) at $0.5 A \cdot g^{-1}$, excellent cycling stability with no capacitance decay over 10000 cycles in H_2SO_4 solution, and good rate performance. In addition, the PC presents high energy density when assembled into symmetric supercapacitors, revealing its applicability in practical applications⁴⁶. Therefore, on the basis of this study, further work could be focused on studying natural materials with abundant heteroatoms (P, N, O, S, and chlorides) and generating other valuable heteroatoms-doped carbons based on them.

Methods

Synthesis of the PC. The cleaned and dried cicada sloughs were ball-milled for 4 h at 600 rpm in a planet-type ball miller. The ball-milled cicada sloughs (1 g) were immersed in 35 mL 50 wt.% H_3PO_4 aqueous solution, stirred for a while to form homogeneous suspension and then transferred into a Teflon-lined stainless steel autoclave and heated at $180^\circ C$ for 12 h. The hydrothermal product was filtered (no washing) and dried at $80^\circ C$. Next, the mixture was heated at $500^\circ C$ for 2 h in N_2 atmosphere at a heating rate of $2^\circ C \cdot min^{-1}$. Finally, the product was thoroughly washed with deionization water until the pH value reached to 7, and further dried at $80^\circ C$ for 12 h. For comparison, the ball-milled cicada sloughs without the H_3PO_4 treatment were pyrolyzed at the same condition, and the product was denoted as PC_{untreated}.

Characterization. The morphology and texture of the materials were characterized by field emission scanning electron microscopy (FESEM) on a Nova NanoSem 450 and field emission transmission electron microscopy (FETEM) on Tecnai G2 F20 S-Twin with acceleration voltage of 200 kV. Elemental compositions of the materials were measured with energy dispersive spectroscopy (EDS) microanalysis attached to the FESEM instrument. X-ray diffraction (XRD) was conducted on a D8 advance Bruker diffractometer with $Cu K_\alpha$ radiation ($\lambda = 1.54056 \text{ \AA}$). Raman spectra were recorded on Renishaw in Via Micro-Raman Spectroscopy. The surface functional groups of the materials were identified by Nicolet iS10 Fourier Transform Infrared (FTIR) Spectrometer using KBr pellets. Nitrogen adsorption-desorption isotherms were measured at 77 K on an AUTOSORB-IQ.

Electrochemical measurements. The working electrodes consist of 80 wt.% active materials, 10 wt.% acetylene black and 10 wt.% polytetrafluoroethylene (PTFE) binder. Then the mixture was coated on a graphite rod (for 1 M H_2SO_4) or a nickel mesh (for 6 M KOH) with a mass loading density of $1 mg \cdot cm^{-2}$, dried in vacuum at $80^\circ C$ for 12 h. In three electrodes systems, the graphite rod (for 1 M H_2SO_4) or nickel mesh (for 6 M KOH) and a saturated calomel electrode (SCE) were used as the counter and reference electrodes, respectively. Cyclic

voltammetry (CV) and electrochemical impedance spectroscopy (EIS) were tested by a CHI400B electrochemical working station. The galvanostatic charge/discharge (GCD) and cycling stability tests were carried out on an automatic LAND battery test instrument^{47,48}.

References

1. Wang, F. X. *et al.* Nanostructured positive electrode materials for post-lithium ion batteries. *Energy Environ. Sci.* **9**, 3570–3611 (2016).
2. Wu, X. W. *et al.* A high-capacity dual core-shell structured MWCNTs@S@PPy nanocomposite anode for advanced aqueous rechargeable lithium batteries. *Nanoscale* **9**, 11004–11011 (2017).
3. Wang, F. X. *et al.* A quasi-solid-state sodium-ion capacitor with high energy density. *Adv. Mater.* **27**, 6962–6968 (2015).
4. Largot, C. *et al.* Relation between the ion size and pore size for an electric double-layer capacitor. *J. Am. Chem. Soc.* **130**, 2730–2731 (2008).
5. Wang, F. X. *et al.* Composites of porous Co₃O₄ grown on Li₂MnO₃ microspheres as cathode materials for lithium ion batteries. *J. Mater. Chem. A* **3**, 4840–4845 (2015).
6. Zhang, L. L. & Zhao, X. S. Carbon-based materials as supercapacitor electrodes. *Chem. Soc. Rev.* **38**, 2520–2531 (2009).
7. Yuan, C. Z. *et al.* Hierarchically structured carbon-based composites: Design, synthesis and their application in electrochemical capacitors. *Nanoscale* **3**, 529–545 (2011).
8. Simon, P. & Gogotsi, Y. Materials for electrochemical capacitors. *Nature* **7**, 845–854 (2008).
9. Frackowiak, E. Carbon materials for supercapacitor application. *Phys. Chem. Chem. Phys.* **9**, 1774–1785 (2007).
10. Rao, C. N. R., Gopalakrishnan, K. & Maitra, U. Comparative study of potential applications of graphene, MoS₂, and other two-dimensional materials in energy devices, sensors, and related areas. *ACS Appl. Mater. Interfaces* **7**, 7809–7832 (2015).
11. Yang, X. W., Cheng, C., Wang, Y. F., Qiu, L. & Li, D. Liquid-mediated dense integration of graphene materials for compact capacitive energy storage. *Science* **341**, 534–537 (2013).
12. Xu, D., Tong, Y., Yan, T. T., Shi, L. Y. & Zhang, D. S. N,P-codoped meso-/microporous carbon derived from biomass materials via a dual-activation strategy as high-performance electrodes for deionization capacitors. *ACS Sustainable Chem. Eng.* **5**, 5810–5819 (2017).
13. Wang, Y. F. *et al.* ZIF-8@MWCNT-derived carbon composite as electrode of high performance for supercapacitor. *Electrochim. Acta* **213**, 260–269 (2016).
14. Yu, X. *et al.* Elucidating surface redox charge storage of phosphorus-incorporated graphenes with hierarchical architectures. *Nano Energy* **15**, 576–586 (2015).
15. Zhang, D. Y. *et al.* Superior supercapacitors based on nitrogen and sulfur co-doped hierarchical porous carbon: Excellent rate capability and cycle stability. *J. Power Sources* **358**, 112–120 (2017).
16. Wei, T. Y., Wei, X. L., Gao, Y. & Li, H. M. Nitrogen, oxygen and phosphorus decorated porous carbons derived from shrimp shells for supercapacitors. *Electrochim. Acta* **169**, 186–194 (2015).
17. Nasini, U. B. *et al.* Phosphorous and nitrogen dual heteroatom doped mesoporous carbon synthesized via microwave method for supercapacitor application. *J. Power Sources* **250**, 257–265 (2014).
18. Ramasahayam, S. K., Hicks, Z. & Viswanathan, T. Thiamine-based nitrogen, phosphorus, and silicon tri-doped carbon for supercapacitor applications. *ACS Sustainable Chem. Eng.* **3**, 2194–2202 (2015).
19. He, C. *et al.* Electrochemically active phosphotungstic acid assisted prevention of graphene restacking for high-capacitance supercapacitors. *Energy Environ. Mater.* **1**, 88–95 (2018).
20. Li, C. Y. *et al.* Fabricating aqueous symmetric supercapacitor with a stable high working voltage of 2 V by using an alkaline-acidic electrolyte. *Adv. Sci.* **6**, 1801665 (2019).
21. Abioye, A. M. & Ani, F. N. Recent development in the production of activated carbon electrodes from agricultural waste biomass for supercapacitors: A review. *Renew. Sust. Energ. Rev.* **52**, 1282–1293 (2015).
22. Gong, C. C. *et al.* Microporous carbon from a biological waste-stiff silkworm for capacitive energy storage. *Electrochim. Acta* **220**, 331–339 (2016).
23. Cheng, P. *et al.* Hierarchically porous carbon by activation of shiitake mushroom for capacitive energy storage. *Carbon* **93**, 315–324 (2015).
24. Ma, F. W., Wan, J. F., Wu, G. & Zhao, H. Highly porous carbon microflakes derived from catkins for high-performance supercapacitors. *RSC Adv.* **5**, 44416–44422 (2015).
25. Ma, G. F. *et al.* White clover based nitrogen-doped porous carbon for a high energy density supercapacitor electrode. *RSC Adv.* **5**, 107707–107715 (2015).
26. Zhang, G. Q. & Zhang, S. T. Characterization and electrochemical applications of a carbon with high density of surface functional groups produced from beer yeast. *J. Solid State Electrochem.* **13**, 887–893 (2009).
27. Qian, W. J. *et al.* Human hair-derived carbon flakes for electrochemical supercapacitors. *Energy Environ. Sci.* **7**, 379–386 (2014).
28. Zhao, Z. H. *et al.* Lignosulphonate-cellulose derived porous activated carbon for supercapacitor electrode. *J. Mater. Chem. A* **3**, 15049–15056 (2015).
29. Qu, J. Y. *et al.* Nitrogen, oxygen and phosphorus decorated porous carbons derived from shrimp shells for supercapacitors. *Electrochim. Acta* **176**, 982–988 (2015).
30. Wu, Y. P., Fang, S. B. & Jiang, Y. Y. Carbon anode materials based on melamine resin. *J. Mater. Chem.* **8**, 2223–2227 (1998).
31. Wang, Y. F. *et al.* Enhancing performance of sandwich-like cobalt sulfide and carbon for quasi-solid-state hybrid electrochemical capacitors. *J. Mater. Chem. A* **5**, 8981–8988 (2017).
32. Wang, S. G. *et al.* Cotton-based hollow carbon fibers with high specific surface area prepared by ammonia etching for supercapacitor application. *RSC Adv.* **4**, 31300–31307 (2014).
33. Kleszyk, P. *et al.* Carbons with narrow pore size distribution prepared by simultaneous carbonization and self-activation of tobacco stems and their application to supercapacitors. *Carbon* **81**, 148–157 (2015).
34. Cordero, D. J., Heras, F., Gilarranz, M. A. & Pinero, E. R. Grape seed carbons for studying the influence of texture on supercapacitor behaviour in aqueous electrolytes. *Carbon* **71**, 127–138 (2014).
35. Jiang, L. *et al.* High rate performance activated carbons prepared from ginkgo shells for electrochemical supercapacitors. *Carbon* **56**, 146–154 (2013).
36. Kumagai, S., Sato, M. & Tashima, D. Electrical double-layer capacitance of micro- and mesoporous activated carbon prepared from rice husk and beet sugar. *Electrochim. Acta* **114**, 617–626 (2013).
37. Li, X. *et al.* Preparation of capacitor's electrode from sunflower seed shell. *Bioresource Technol.* **102**, 1118–1123 (2011).
38. Fan, Y. *et al.* Micro-mesoporous carbon spheres derived from carrageenan as electrode material for supercapacitors. *J. Power Sources* **268**, 584–590 (2014).
39. Bichat, M. P., Pinero, E. R. & Beguin, F. High voltage supercapacitor built with seaweed carbons in neutral aqueous electrolyte. *Carbon* **48**, 4351–4361 (2010).
40. Zhu, H., Wang, X. L., Yang, F. & Yang, X. R. Promising Carbons for Supercapacitors Derived from Fungi. *Adv. Mater.* **23**, 2745–2748 (2011).

41. Wu, Y. P., Rahm, E. & Holze, R. Effects of heteroatoms on electrochemical performance of electrode materials for lithium ion batteries. *Electrochim. Acta* **47**, 3491–3507 (2002).
42. Wang, D. B., Geng, Z., Li, B. & Zhang, C. M. High performance electrode materials for electric double-layer capacitors based on biomass-derived activated carbons. *Electrochim. Acta* **173**, 377–384 (2015).
43. Wang, Q. *et al.* A high-capacity carbon prepared from renewable chicken feather biopolymer for supercapacitors. *J. Power Sources* **225**, 101–107 (2013).
44. Farma, R. *et al.* Preparation of highly porous binderless activated carbon electrodes from fibres of oil palm empty fruit bunches for application in supercapacitors. *Bioresource Technol.* **132**, 254–261 (2013).
45. He, X. J. *et al.* Rice husk-derived porous carbons with high capacitance by ZnCl₂ activation for supercapacitors. *Electrochim. Acta* **105**, 635–641 (2013).
46. Li, C. Y. *et al.* Fabricating aqueous symmetric supercapacitor with a stable high working voltage of 2 V by using an alkaline-acidic electrolyte. *Adv. Sci.*, 1801665 (2018).
47. Jia, H. Y., Sun, J. W., Xie, X., Yin, K. B. & Sun, L. T. Cicada slough-derived heteroatom incorporated porous carbon for supercapacitor: Ultra-high gravimetric capacitance. *Carbon* **143**, 309–317 (2019).
48. Pandolfo, A. G. & Hollenkamp, A. F. Carbon properties and their role in supercapacitors. *J. Power Sources* **157**, 11–27 (2006).

Acknowledgements

Financial support from National Materials Genome Project (2016YFB0700600), Distinguished Young Scientists Program of NSFC (51425301, 21374021, 51673096 and U1601214), Research Foundation of State Key Lab (ZK201805), and Jiangsu Distinguished Professorship Program (2016), and Sanyo Chem. Co. Ltd. is greatly appreciated.

Author Contributions

W.W. suggested this topic and collected some samples. B.C. carried out the electrochemical experiments. B.C., Y.W., W.W., C.L. and Y.Z. analyzed and discussed the results. B.C., Y.W. and C.L. wrote the manuscript. L.F., Y.Z., L.Z. and Y.W. supervised the research project.

Additional Information

Supplementary information accompanies this paper at <https://doi.org/10.1038/s41598-019-41769-y>.

Competing Interests: The authors declare no competing interests.

Publisher's note: Springer Nature remains neutral with regard to jurisdictional claims in published maps and institutional affiliations.



Open Access This article is licensed under a Creative Commons Attribution 4.0 International License, which permits use, sharing, adaptation, distribution and reproduction in any medium or format, as long as you give appropriate credit to the original author(s) and the source, provide a link to the Creative Commons license, and indicate if changes were made. The images or other third party material in this article are included in the article's Creative Commons license, unless indicated otherwise in a credit line to the material. If material is not included in the article's Creative Commons license and your intended use is not permitted by statutory regulation or exceeds the permitted use, you will need to obtain permission directly from the copyright holder. To view a copy of this license, visit <http://creativecommons.org/licenses/by/4.0/>.

© The Author(s) 2019